# Magnetic anisotropy of single-crystal antiperovskite $Mn_3GaC$ studied by ferromagnetic resonance and dynamic magnetic-response simulations

F. Scheibel
*Materialwissenschaft, Technische Universität Darmstadt, 64287 Darmstadt, Germany*

B. Zingsem, T. Feggeler, R. Meckenstock, D. Spoddig, M. Farle, and M. Acet
*Fakultät für Physik, Universität Duisburg-Essen, D-47048 Duisburg, Germany*

(Received 22 October 2017; revised manuscript received 25 March 2019; published 13 May 2019)

The Mn-based antiperovskite $Mn_3GaC$ is an interesting material for magnetocaloric cooling applications below room temperature. To optimize its use, knowledge of the anisotropic magnetic properties is required. Here, we use a single crystal to study the magnetic anisotropy by the ferromagnetic resonance technique and magnetic-response simulations. The anisotropy constant $K_4 = -5.49$ kJ/m$^3$ obtained in combination from experiment and simulations is about an order of magnitude smaller than that of bcc Fe. The magnetically soft nature of this material practically in all crystallographic directions is favorable for using it in polycrystalline form for magnetic refrigeration.

DOI: 10.1103/PhysRevMaterials.3.054403

## I. INTRODUCTION

Cooling and warming by making use of the magnetocaloric effect (MCE) is an environmentally friendly way to attain and maintain a desired temperature over the use of the conventional gas-compression method, which involves environmentally harmful gasses [1,2]. Currently, the broadest interest lies in cooling around room temperature mainly for household refrigeration and air-conditioning. However, the effect is also interesting for applications in the temperature range between room and liquid-helium temperatures, in particular to replace the use of helium, the sources of which are gradually depleting [3,4]. However, the working-temperature range of a given magnetocaloric material is limited at most to a few tens of degrees, so that a range of materials with complementing working ranges have to be employed together to be able to reach and maintain a targeted temperature.

Refrigeration applications at low temperatures cover a broad range extending from scientific research to food and tissue preservation. Two classes of materials and their derivatives are particularly interesting for applications below room temperature. One is the antiperovskite $Mn_3GaC$ and its nitrogen-substituted modifications $Mn_3Ga(C, N)$ [5–7]. The other is the $(Mn, Cr)_2Sb$-based pnictide and its modifications obtained by substituting other 3*d* elements for Cr and other main group elements for Sb [8,9]. The antiperovskites operate in a temperature range $130 \leqslant T \leqslant 160$ K, and the Mn-based pnictides cover the range $150 \leqslant T \leqslant 320$ K, making it worthwhile to study these systems in more detail.

Further detailed studies of these systems would involve looking closer at element-specific and crystallographic properties and how these properties become involved in the making up of the features observed in the magnetic properties. Here we focus on the $Mn_3GaC$, for which we have successfully obtained a single crystal making it possible to investigate and resolve the properties with respect to crystal orientation.

$Mn_3GaC$ undergoes a first-order magnetostructural transition from a low-temperature antiferromagnetic (AF) to a high-temperature ferromagnetic (FM) phase at $T_i = 165$ K and a second-order magnetic transition from the FM to the paramagnetic (PM) phase at the Curie temperature $T_C = 246$ K [10]. $Mn_3GaC$ in the AF state has a cubic $Pm\text{-}3m$ symmetry with a lattice parameter $a = 0.389$ nm [11]. The magnetostructural transition from the AF to the FM state is accompanied by a volume change of about 0.5% without a change in the crystal symmetry. The transition can be induced by magnetic field, pressure, or temperature [12–15]. This material has been in focus in recent years because of the large MCE and giant magnetoresistance observed around the transition [5,16,17].

Regarding the MCE, a narrow transitional hysteresis and a large magnetic-field shift of the transition temperature are favorable for attaining a large and reversible adiabatic temperature change $\Delta T_{ad}$ [6,18,19]. Additionally, a sharp transition along with the narrow transitional hysteresis would enable a reversible $\Delta T_{ad}$ even in low magnetic fields. The fastest change of the magnetization with respect to magnetic field can be obtained by applying the field along the magnetization easy axis, so that it would be necessary to know what the magnetically anisotropic properties are. Even if it would be difficult to employ single crystals in a magnetic refrigerator as the active material, knowledge of the magnetic anisotropy could be useful for obtaining quasi-single-crystals by directional solidification along a favorable, magnetically soft crystallographic orientation. Directionally solidified materials can be more readily prepared than their single crystals and thus used in magnetic refrigerators by orienting them appropriately with respect to the applied field, making the refrigeration more efficient. Therefore, in all cases it is necessary to know the magnetic anisotropy of any system that is to be designed for use in a magnetic refrigerator for optimization purposes. Here we focus on a single crystal of the low-temperature

 ©2019 American Physical Society

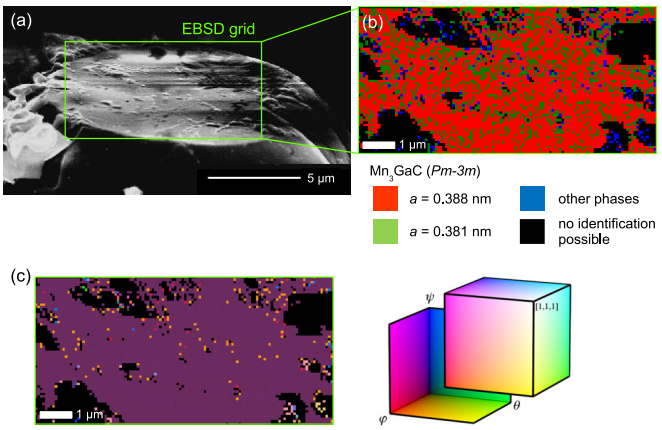


FIG. 1. Characterization of the crystal. (a) SEM image of the surface of the $Mn_3GaC$ crystal. The green frame shows the area of the EBSD analysis in (b). (b) $120 \times 60$ $\mu m^2$ EBSD grid with 0.08 $\mu m^2$ resolution. The color-code corresponds to the identified phases given in the legend. (c) EBSD grid for crystal orientation. The uniform violet-colored region indicates constant Euler angles so that the crystal surface is determined to be a (100) plane after taking into account the tilt of the surface with respect to the detector. The color code of the Euler angles and crystal orientation directions corresponds to the representation used in Ref. [21]. The crystal is represented by the cube in the legend.

magnetocaloric material $Mn_3GaC$ grown by self-fluxing [20], and we estimate the magnetocrystalline anisotropy energy (MCAE) using ferromagnetic resonance (FMR) and a single-crystal sample.

## II. EXPERIMENT

A target stoichiometry of $Mn_4Ga_2C$ was initially prepared by mixing the components and allowing it to undergo a solid-state reaction in its powder form. After the first firing at 800 °C, the sintered powder was ground and pressed into a pellet and reintroduced into the furnace at 800 °C. The procedure was repeated three times, after which the material was inspected. A scanning electron microscope (SEM) was used for electron backscatter diffraction (EBSD) and energy-dispersive x-ray spectroscopy (EDX) studies. Within the obtained material, some grains appeared to have a single-crystalline morphology. Such a grain of size $15 \times 15 \times 28$ $\mu m^3$ produced by self-fluxing was selected and was verified by EBSD to be largely a single crystal. The composition of the sample was determined by EDX. The orientation was also determined by EBSD, which also verified the antiperovskite *Pm-3m* crystal symmetry. This particular single crystal was used in all of the experiments described in this work. For the FMR measurements, the sample was transported and mounted using the same sample holder used in the EBSD studies, so that the crystal orientation was preserved when the sample was mounted in the instrument cavity.

Figure 1 shows the results of the EBSD studies. Due to the small size of the sample, no surface treatment was done. The investigated surface is shown in Fig. 1(a) bounded by the green rectangle. Figure 1(b) shows the phase map and the obtained lattice parameters resulting from the EBSD analysis.

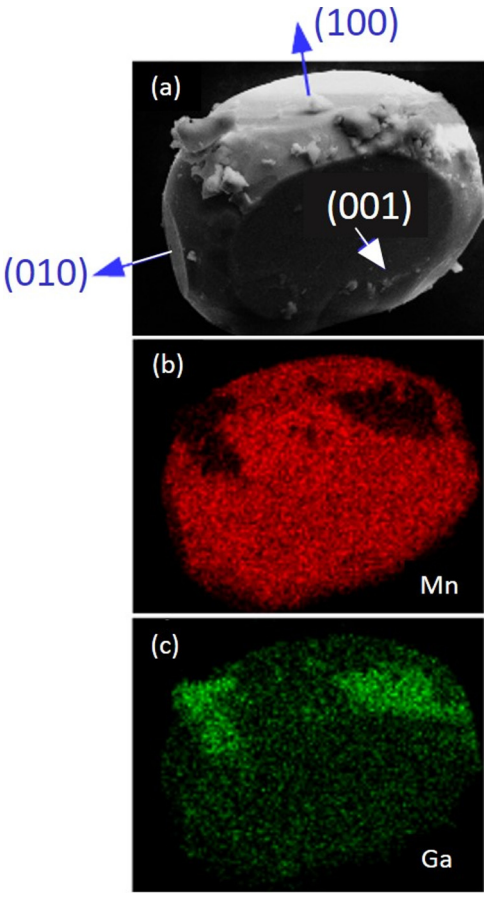


FIG. 2. SEM images showing (a) the truncated prismatic $Mn_3GaC$ single crystal with {100} main surfaces. Small pieces of a Ga-rich phase are found mainly at the edges. (b) EDX mapping for the Mn $K\alpha 1$ (red) and (c) Ga $K\alpha 1$ emissions (green).

Using the space group *Pm-3m*, we find the lattice parameters 0.381 and 0.386 nm, which are close to the cubic lattice parameter 0.3896 nm of $Mn_3GaC$ [12]. The variation in the lattice parameter is expected to be due to imperfections on the untreated surface. In spite of the imperfections, the range in which the lattice constants lie suggests that the surface is single crystalline with a (100) plane. Figure 1(c) shows the color-coded crystal orientation [21]. The uniformity of the color indicates constant Euler angles providing further evidence for the single crystallinity.

Figure 2 shows the results of the SEM studies. Figure 2(a) is an image of the crystal showing that it is a truncated rectangular prism with the surfaces as {100} planes. Some droplets also form at the face edges. EDX mappings for Mn $K\alpha 1$ and Ga $K\alpha 1$ emissions are shown in Figs. 2(b) and 2(c), respectively. The mapping locates a Mn-rich [Fig. 2(b)] phase at the surfaces and a Ga-rich phase at the positions of the larger droplets on the corners [Fig. 2(c)]. The Mn-rich and Ga-rich phases are identified as $Mn_3GaC$ and $Mn_2Ga_5$, respectively. The latter is FM with $T_C = 440$ K [22].

The temperature dependence of the magnetization $M(T)$ was measured with a superconducting quantum interference device magnetometer in the range $10 \leqslant T \leqslant 300$ K. For FMR studies, the sample was mounted on a goniometer using

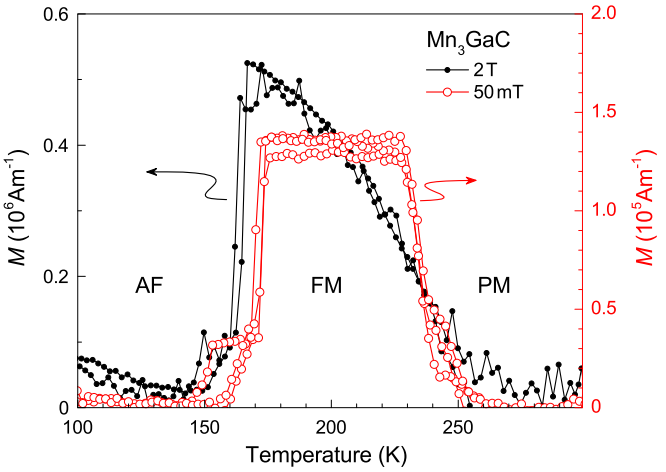


FIG. 3. $M(T)$ of $Mn_3GaC$ single crystal in a field of 50 mT (red) and 2 T (black). Dashed blue lines mark the temperatures at which angular-dependent FMR spectra are measured.

carbon tape. The experiments were carried out in the range $100 \leqslant T \leqslant 300$ K in a Varian TE102 cavity with an eigenfrequency of 9.238 GHz. A maximum modulation of 1.5 mT at 100 kHz was used, and the measurement was conducted using an electron paramagnetic resonance spectrometer incorporating an X-Band bridge. The cavity is located between the poles of an electromagnet where the maximum magnetic field is 1.6 T.

## III. RESULTS AND DISCUSSION

### A. Magnetization

Figure 3 shows $M(T)$ of the single crystal in an applied field of 50 mT (red) and 2 T (black). A background signal arising from FM $Mn_2Ga_5$ and the PM carbon tape used in fixing the sample has been subtracted in both the 5 mT and the 5 T data. The FM/PM transition is at $T_C = 236$ K with no thermal hysteresis, and the AF/FM magnetostructural transition is at $T_i = 163$ K with a thermal hysteresis of about 3 K. The absolute value of the magnetization was then scaled to the known $M(T)$ value at $T_i$ [6]. $T_i$ shifts with applied field by about 5 K $T^{-1}$. Below $T_C$, $M(T)$ measured in 5 mT reaches the demagnetization limit so that it is temperature-independent down to $T_i$. The measurement under 5 T shows a mean-field behavior down to $T_i$. The behavior of $M(T)$ is in agreement with previous measurements on $Mn_3GaC$ powder samples [6,10,18].

### B. Ferromagnetic resonance

The FMR absorption derivative spectra, $\partial(\mathrm{FMR})_{\mathrm{abs}}/\partial B$, for $150 \leqslant T \leqslant 270$ K at 0° are shown in Fig. 4. The electron spin resonance (ESR) position is located at 0.332 T, and a strong signal is associated with it ranging beyond the vertical scale of the plot as shown in Fig. 4(a). This is mainly related to the carbon tape used for sample-mounting. Features corresponding to fields below the ESR line are related to FM $Mn_2Ga_5$. These features, making up the background signal, are essentially temperature-independent up to 270 K since the

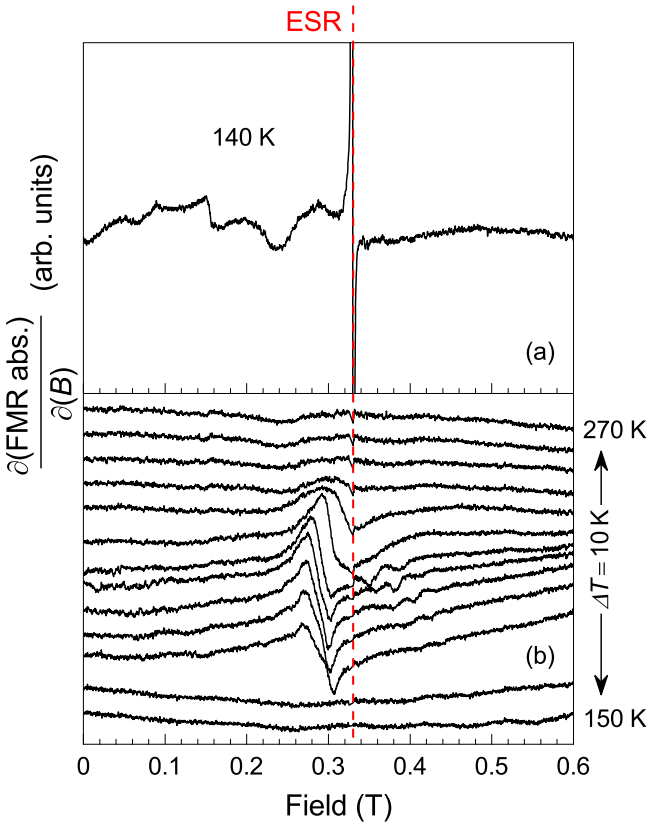


FIG. 4. Field dependence of the FMR absorption derivative. (a) The raw data at 140 K including features related to the presence of the $Mn_2Ga_5$ impurity phase and a strong ESR line at 0.332 T ranging beyond the vertical scale. The strong ESR line is mainly due to the carbon tape used for sample-mounting. There is no FMR related to $Mn_3GaC$ at 140 K since it is AF at this temperature. (b) The FMR absorption derivative for different temperatures around $T_i = 163$ K at 0°. All spectra are subtracted from the 140 K spectra in part (a) to eliminate the ESR and background signals.

saturation magnetization of $Mn_2Ga_5$ is weakly temperature-dependent due to its higher-lying $T_C$ at 440 K. All spectra shown in Fig. 4(b) have been subtracted from the 140 K spectra to eliminate the ESR and the FM background signals. At 150 and 160 K, the sample is AF (cf. Fig. 3) and no FMR is observed. For $T > T_i$, the sample is FM, and FMR begins to be observed at 170 K at 0.289 T. At 220 and 230 K, FMR shifts toward the ESR position at a rate of 0.6 mT $K^{-1}$ as the temperature approaches $T_C$ [23]. For $T \geqslant 250$ K, the sample is PM, and FMR is no longer observed.

Other than the FMR around 0.289 T seen in Fig. 4(b), two further resonances occur for $T > T_i$ in the field range $0.330 \leqslant B \leqslant 0.463$ T. These weaker resonances are expected to be related to edge modes [24]. The positions of these resonances shift progressively at a rate of $-2.2$ mT $K^{-1}$ toward the ESR position with increasing temperature. Edge-mode resonances depend more strongly on the magnitude of the MCAE than the uniform FMR mode does, accounting for the observed faster shift of the nonuniform edge modes with increasing temperature [23]. For $T > 220$ K, nonuniform excitations are no longer observed due to the overlap with the ESR and the main FMR.

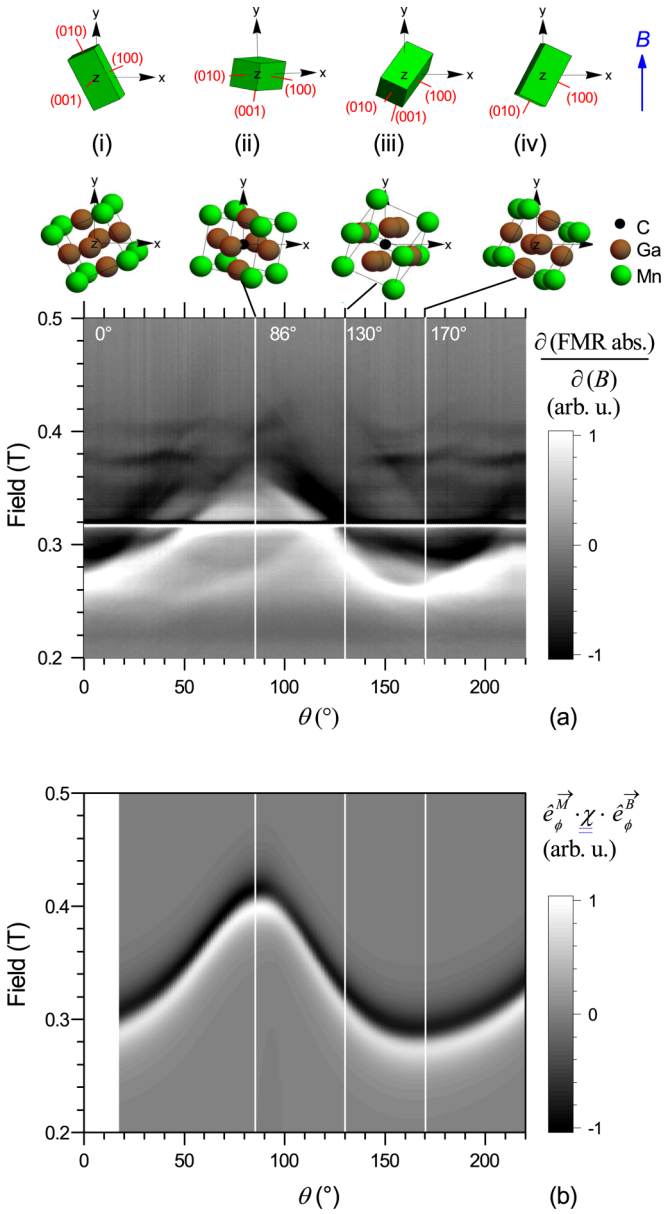


FIG. 5. Angular dependence of FMR. (a) Angular dependence of FMR absorption derivative in gray scale measured at 200 K in the FM state. Parts (i)–(iv) show the orientation of the faces of the crystal and the orientation of the cell for the characteristic rotation angles 0°, 68°, 130°, and 170°. The selected coordinate system for the experimental geometry is included in (i)–(iv). (b) Calculated angular dependence of the amplitude of $\hat{e}_{\phi}^{\vec{M}} \cdot \underline{\underline{\chi}} \cdot \hat{e}_{\phi}^{\vec{B}}$ in gray scale. The simulated data are shifted by 18° to comply with the initial orientation of the sample in the spectrometer shown in part (a), (i).

We determine the magnetic anisotropy by angular-dependent FMR measurements and dynamic magnetic response simulations, for which the results are shown in Fig. 5. The magnetic anisotropy is composed of the MCAE and the shape anisotropy energy SAE of the crystal.

Angular-dependent and field-dependent FMR spectra at 200 K are shown in Fig. 5(a). The crystal is rotated around the $x$-axis from $\theta = 0°$ to 220° in steps of 1°. The coordinate system for the experimental geometry of the spectrometer is included in Fig. 5(a), (i)–(iv). The magnetic field **B** is along the $y$-direction. The orientation of the sample and the unit cell at several characteristic angles are shown in Fig. 5(a), (i)–(iv). At the start of the rotation ($\theta = 0°$), the longer axis of the crystal lies at 26° away from the $y$-axis and 13° from the $z$-axis [Fig. 5(a), (i)]. This offset is due to the original positioning of the crystal in the sample holder when used for the EBSD measurements. The crystal was transferred to the FMR spectrometer and placed inside the cavity without repositioning it. Further orientations for $\theta = 86°$, 130°, and 170° are shown in Figs. 5(a), (ii)–(iv) as the crystal is progressively rotated. $\partial(\mathrm{FMR})_{\mathrm{abs}}/\partial B$ in Fig. 5, (i) is shown on a gray scale. The ESR of the carbon tape at 0.322 T is independent of temperature and angle.

The FMR data in Fig. 5(a) have a twofold symmetry and oscillate between 0.24 and 0.38 T. The angular shift of the FMR is dominated by the SAE of the crystal. At 0° and 170°, where minima are observed, the long axis of the crystal points closer to the direction of the magnetic field. At 86°, a maximum occurs since the short axis [Fig. 5(a), (ii)] is now nearly along the field direction. The influence of the MCAE is observed as an asymmetry centered around the minimum at $\theta = 160°$ and in the range $130° \leqslant \theta \leqslant 190°$. At 130°, the MCAE is minimum due to the nearly parallel orientation of the (111) direction to $\vec{B}$ [Fig. 5(a), (iii)]. In combination with the decrease of the SAE from 86° to 130°, a strong decrease of the resonance field can be observed. At 170°, the SAE is minimum but not the MCAE since the (110) direction points in the direction of the field at this angle. This results in a slower increase of the resonance field toward higher angles with increasing field, leading to an asymmetric curve around the minimum.

### C. Modeling of FMR

We analyze the spectra in Fig. 5(a) using a general analytical solution of the Landau-Lifschitz-Gilbert equation [25,26]

$$\partial \mathbf{M}/\partial t = -\gamma \mathbf{M} \times \mathbf{B}_{\mathrm{eff}} - \frac{\alpha}{M_s}(\mathbf{M} \times \partial \mathbf{M}/\partial t), \qquad (1)$$

where $\gamma$ is the gyromagnetic ratio, **M** is the magnetization, $\mathbf{B}_{\mathrm{eff}}$ is the effective magnetic field, and $\alpha$ is the damping parameter. The effective magnetic field is described by

$$dF = -\mathbf{B}_{\mathrm{eff}} \cdot d\mathbf{M}, \qquad (2)$$

where the free energy $F$ is expressed as

$$F = \tfrac{1}{4}K_4\left(\alpha_1^2\alpha_2^2 + \alpha_1^2\alpha_3^2 + \alpha_2^2\alpha_3^2\right) + \tfrac{1}{2}\mu_0 \mathbf{M} \cdot \underline{\underline{N}} \cdot \mathbf{M} - \mathbf{M} \cdot \mathbf{B}. \qquad (3)$$

Here, $\underline{\underline{N}}$ is the demagnetization tensor assuming an ellipsoidal sample with an aspect ratio of 15/28 [27]. We assume a fourfold crystalline anisotropy $K_4$ due to the cubic structure of the compound. $\alpha_i$ are the direction cosines.

The solutions of Eqs. (1) and (2) give the nonlinearized high-frequency susceptibility tensor $\underline{\underline{\chi}}_{hf}$ given in its Jacobian matrix form as [Eq. (9) in [27]]

$$\underline{\underline{\chi}}_{\mathrm{hf}} = -\left((\underline{\underline{J}}_{\mathbf{m}})^{-1} \cdot \underline{\underline{J}}_{\mathbf{b}}\right), \qquad (4)$$

where $\underline{\underline{J}}_{\mathbf{m}}$ and $\underline{\underline{J}}_{\mathbf{b}}$ are the Jacobian matrices in magnetization $\mathbf{m}$ and microwave magnetic field $\mathbf{b}$, respectively. The measured field derivative of the FMR absorption is then proportional to the projection of $\underline{\underline{\chi}}_{\mathrm{hf}}$ in the direction of $\mathbf{m}$ and $\mathbf{b}$ and can be written as

$$\partial(\mathrm{FMR})_{\mathrm{abs}}/\partial B \propto \hat{\mathbf{e}}_{\phi}^{\mathbf{m}} \cdot \partial \underline{\underline{\chi}}/\partial B \cdot \hat{\mathbf{e}}_{\phi}^{\mathbf{b}}. \tag{5}$$

The projection given in Eqs. (4) and (5) has the advantage that no linearization is needed, and thus all possible excitations are included in the calculated spectra except the edge modes. A value $K_4 = -5.49 \pm 0.05$ kJ m$^{-3}$ gives the best agreement of the spectra in Fig. 5(a) with the calculated spectra in Fig. 5(b). Figure 5(b) exhibits a twofold symmetry of the amplitude in the angular range $0^\circ \leqslant \theta \leqslant 220^\circ$ confirming the dominant shape anisotropy as compared to the weaker magnetocrystalline anisotropy. The FMR varies between 0.26 and 0.41 T, which agrees with the measured spectra in Fig. 5(a). The calculated spectra are shifted by 15° to higher angles to match the experimental data in Fig. 5(a). The 15° shift is very close to the 13° angular offset of the sample with respect to the $y$-axis [cf. Fig. 5(a), (i)]. Any difference can be due to uncertainties in the orientation of the sample with respect to the magnetic field. The influence of MCAE becomes evident in the broadening of the FMR minimum in the range $130^\circ \leqslant \theta \leqslant 190^\circ$. This allows us to identify the [111] direction as the magnetic easy axis and the [100] direction as the hard axis, in agreement with the results of previous studies on polycrystalline samples [10]. The absence of studies on single crystals does not allow a comparison. The estimated value is an order of magnitude smaller than that of bcc Fe [28,29]. Therefore, an appreciable anisotropy in the magnetocaloric effect would not be expected since the magnetization process would be nearly equivalent in both the easy and hard axis. This property is favorable for the use of polycrystalline material for magnetocaloric refrigeration since all grains would magnetize with the same process.

## IV. CONCLUSION

Knowledge of the magnetic anisotropy in magnetocaloric materials is necessary to optimize the crystallographic orientation of the material with respect to the applied field for effective refrigeration. The Mn-based antiperovskite $Mn_3GaC$ being an interesting material for magnetocaloric applications below room temperature, we have studied the magnetic anisotropy using ferromagnetic resonance and magnetic-response simulations on a single-crystal specimen. The anisotropy is estimated to be $K_4 = -5.49$ kJ/m$^3$ with an easy axis along the [111] direction. The magnetically soft nature of this material is favorable for use in magnetic refrigeration in its polycrystalline form.

## ACKNOWLEDGMENTS

We thank Markus Gruner and Michael Winkelhofer for useful discussions. This work was supported by the Deutsche Forschungsgemeinschaft (SPP 1599).

[1] A. Planes, L. Mañosa, and M. Acet, J. Phys.: Condens. Matter **21**, 233201 (2009).
[2] N. R. Ram, M. Prakash, U. Naresh, N. S. Kumar, T. S. Sarmash, T. Subbarao, R. J. Kumar, G. R. Kumar, and K. C. B. Naidu, J. Supercond. Nov. Magn. **31**, 1971 (2018).
[3] K. Das, J. Magn. Magn. Mater. **458**, 52 (2018).
[4] L. C. Wang, Q. Y. Dong, Z. J. Mo, Z. Y. Xu, F. X. Hu, J. R. Sun, and B. G. Shen, J Appl. Phys. **114**, 163915 (2013).
[5] T. Tohei and H. Wada, J. Appl. Phys. **94**, 1800 (2003).
[6] Ö. Çakır and M. Acet, Appl. Phys. Lett. **100**, 202404 (2012).
[7] Ö. Çakır and M. Acet, J. Magn. Magn. Mater. **344**, 207 (2013).
[8] L. Caron, X. F. Miao, J. C. P. Klaasse, S. Gama, and E. Brück, Appl. Phys. Lett. **103**, 112404 (2013).
[9] A. Tekgül, Ö. Çakır, M. Acet, M. Farle, and N. Ünal, J. Appl. Phys. **118**, 153903 (2015).
[10] D. Fruchart and E. F. Bertaut, J. Phys. Soc. Jpn. **44**, 781 (1978).
[11] D. Fruchart, E. F. Bertaut, F. Sayetat, M. Nasr Eddine, R. Fruchart, and J. P. Sénateur, Solid State Commun. **8**, 91 (1970).
[12] J.-P. Bouchaud, R. Fruchart, R. Pauthenet, M. Cuillot, H. Bartholin, and F. Chaisé, J. Appl. Phys. **37**, 971 (1966).
[13] T. Kaneko, T. Kanomata, C. Miura, G. Kido, and Y. Nakagawa, J. Magn. Magn. Mater. **70**, 261 (1987).
[14] T. Kaneko, T. Kanomata, and K. Shirakawa, J. Phys. Soc. Jpn. **56**, 4047 (1987).
[15] Ö. Çakır, M. Acet, M. Farle, and A. Senyshyn, J. Appl. Phys. **115**, 043913 (2014).
[16] O. Gutfleisch, M. A. Willard, E. Brück, C. H. Chen, S. G. Sankar, and J. P. Liu, Adv. Mater. **23**, 821 (2011).
[17] A. M. Tishin and Y. I. Spichkin, Int. J. Refrig. **37**, 223 (2014).
[18] F. Scheibel, T. Gottschall, K. Skokov, O. Gutfleisch, M. Ghorbani-Zavareh, Y. Skourski, J. Wosnitza, Ö. Çakır, M. Farle, and M. Acet, J. Appl. Phys. **117**, 233902 (2015).
[19] I. Titov, M. Acet, M. Farle, D. Gonzalez-Alonso, L. Mañosa, A. Planes, and T. Krenke, J. Appl. Phys. **112**, 073914 (2012).
[20] P. C. Canfield and Z. Fisk, Philos. Mag. B **65**, 1117 (1992).
[21] G. Nolze, Cryst. Res. Technol. **50**, 188 (2015).
[22] S. Kim, M. Boström, and D. Seo, J. Am. Chem. Soc. **130**, 1384 (2008).
[23] R. Meckenstock, K. Harms, O. von Geisau, and J. Pelzl, J. Magn. Magn. Mater. **148**, 139 (1995).
[24] R. D. McMichael and B. B. Maranville, Phys. Rev. B **74**, 024424 (2006).
[25] L. D. Landau and E. M. Lifshitz, Phys. Z. Sowjetunion **8**, 153 (1935).
[26] T. L. Gilbert, IEEE Trans. Magn. **40**, 3443 (2004).
[27] B. W. Zingsem, M. Winklhofer, R. Meckenstock, and M. Farle, Phys. Rev. B **96**, 224407 (2017).
[28] C. J. Tung, I. Said, and G. E. Everett, J. Appl. Phys. **53**, 2044 (1982).
[29] S. V. Halilov, A. Ya. Perlov, P. M. Oppeneer, A. N. Yaresko, and V. N. Atonov, Phys. Rev. B **57**, 9557 (1998).